Cement and Concrete Research 55 (2014) 1–13

Contents lists available at ScienceDirect

Cement and Concrete Research

journal homepage: http://ees.elsevier.com/CEMCON/default.asp

Durability of an Ultra High Performance Fiber Reinforced Concrete (UHPFRC) under progressive aging

Wei Wang [a,1], Jian Liu [b], Franck Agostini [b,*], Catherine A. Davy [b], Frédéric Skoczylas [b], Dominique Corvez [c]

[a] Key Laboratory of Ministry of Education for Geomechanics and Embankment, and Engineering Geotechnical Research Institute, Hohai University, 1 Xikang Road, Nanjing 210098, China
[b] Laboratoire de Mécanique de Lille (LML) UMR CNRS 8107, and Ecole Centrale de Lille, CS20048, F-59651 Villeneuve d'Ascq Cedex, France
[c] Lafarge Group, 61 Rue des Belles Feuilles, BP40, F-75782 Paris Cedex 16, France

ARTICLE INFO

Article history:
Received 2 October 2012
Accepted 6 September 2013

Keywords:
High performance concrete (E)
Fiber reinforcement (E)
Permeability (C)
Durability (C)
Aging (C)
Bending strength (C)

ABSTRACT

We assess the durability of an Ultra High Performance Fiber Reinforced Concrete (UHPFRC) after accelerated aging, i.e. after partial drying, or 105 °C oven-drying (dry reference state), 200, 300 or 400 °C heat-treatment, or progressive splitting (Brazilian test). Our key experimental tool is gas permeability K_{gas} under varying confinement P_c, coupled to MIP and SEM analysis. UHPFRC properties are compared to standard mortar and ordinary concrete.

Whereas usual UHPFRCs involve pozzolanic additions and thermal curing, this UHPFRC does not, and is significantly more porous (by 9–10%). However, 74% of its porosity comprises pores smaller than 4 nm, i.e. located within the C–S–H. Dry reference state UHPFRC lies in the range of very high durable materials, with an average $K_{gas} = 10^{-18}$ m^2. Damage by heat-treatment at 400 °C induces limited de-bonding at the fiber/paste interface, which increases K_{gas} up to 10^{-17} m^2 at $P_c = 6$ MPa. While sustaining more than 300 μm/m tensile strain, K_{gas} of UHPFRC remains virtually identical.

1. Introduction

1.1. Industrial and scientific context

Currently, France has the second nuclear power plant industrial park (behind USA), with as many as 58 independent reactors spread around the country. 24 of these reactors belong to the so-called Second Generation, which was built between 1970 and 1988 (i.e. they are between 25 and 43 years old). Each reactor unit of the Second Generation comprises a containment building, which is made of two superposed reinforced concrete structures. Their aim is to act as a barrier against any aircraft strike, and also as a tight container, should any leakage of the reactor vessel occur. In such event, gas pressure build-up is expected inside the containment structure, which should not spread through to the environment. Contrary to the Second Generation reactors, containment buildings of the First Generation reactors are made of a non porous steel casing superposed to a concrete container, which generates different safety issues.

The French law (on transparency and safety of nuclear operation systems, June 13th, 2006) imposes that, every ten years, all French nuclear reactors are stopped in turn, and fully test-proofed, in order to check if they are fit to be operated for ten more years. In particular, the tightness of Second Generation reactors to gas pressure is ascertained as follows: an internal gas pressure is applied to the containment building, at a conventional rate and amplitude, so that the reactor is declared fit for an extended operation if the leakage rate is below a regulatory-fixed value.

Electricité de France (EDF), the first French electricity operating company, anticipates novel methods for lengthening the operating duration of its oldest reactors, among which are the 25–43 years old Second Generation ones. A foreseen path is to strengthen the tightness of containment buildings, which has degraded with time, due to concrete drying and aging (marked by various crack patterns), and to prestress decrease. As recalled by Ozyildirim [1], one method of improving durability is to lower the permeability of concrete. One viable option is to cover the extrados of the current concrete buildings with a supplementary concrete layer, aimed at increasing its tightness for at least 30 more years.

In this context, a specific Ultra High Performance Fiber Reinforced Concrete (UHPFRC), developed by Lafarge company, is being considered under the form of pre-cast slabs, assembled and glued together (with a specific mortar) on the existing structures. This novel material is a cheaper version of the commercial Reactive Powder Concretes of the Ductal™ range (also known as UHPFRC-D) [2–4], owing to its simpler manufacturing process. Its requirement specifications comprise good long-term adherence (yet, this issue is not addressed here), and adequate durability performance. Similarly to Ductal™, this UHPFRC is a self-compacting concrete, and it possesses a recognized high mechanical performance, with a compressive strength above 120 MPa, a tensile

* Corresponding author. Tel.: +33 320 676027.
E-mail address: Franck.agostini@ec-lille.fr (F. Agostini).
[1] Tel.: +86 25 83787561.

0008-8846/$ – see front matter © 2013 Elsevier Ltd. All rights reserved.
http://dx.doi.org/10.1016/j.cemconres.2013.09.008

strength above 5–6 MPa, a porosity (measured with water) below 10%, remarkable ductility provided by metallic fiber presence, and an excellent resistance to chloride penetration [2,5].

1.2. Investigation of durability through gas permeability experiments

Concrete durability performance is generally assessed by a number of parameters, among which mechanical properties and gas permeability are key [1,6]. In a publication aimed at the French concrete industry, V. Baroghel–Bouny [7] proposes a classification of durable concretes wrt. a number of indicators, among which are gas permeability and porosity, which are based on extensive experimental investigations, see Table 1. Very high durability corresponds to (1) apparent gas permeability at values below 10^{-17} m^2 (measured after drying at 105 °C with a gas pressure gradient on the order of 2 MPa), while (2) corresponding porosity P_{water} (measured by water saturation) is of 6 to 9%, and porosity P_{hg} (measured by mercury intrusion porosimetry—MIP) is of 3 to 6%. Other key indicators include chloride diffusion coefficients and electrical resistivity, yet these are not the focus of the present contribution.

A number of experiments have been conducted in our laboratory on damaged Civil Engineering materials: these have shown that gas permeability K_{gas} is very sensitive to the closure of either macro-cracks [8] or micro-cracks [9,10]. Applying a hydrostatic stress (or confining pressure P_c) to a damaged porous sample induces a closure (or an aperture upon unloading), which, in turn, produces a characteristic hydraulic behavior, see Fig. 1.

Table 1
Classification and (indicative) limit values for general (G) or substitution (S) durability indicators: porosity, electrical resistivity, diffusion coefficient and permeability, as translated from [7]. Concrete type is given on an indicative basis.

		Classification and limit values				
	Potential durability indicator	Very low	Low	Average	High	Very high
G	Porosity accessible to water (%) P_{water}	>16	14 to 16	12 to 14	9 to 12	6 to 9
S	Porosity measured by mercury intrusion (%) P_{Hg}		13 to 16	9 to 13	6 to 9	3 to 6
S	Electrical resistivity (Ohm·m)	<50	50 to 100	100 to 250	250 to 1000	>1000
G	Effective chloride diffusion coefficient (10^{-12} $m^2.s^{-1}$) Deff	>8	2 to 8	1 to 2	0.1 to 1	<0.1
G	Apparent chloride diffusion coefficient (measured by a migration test) (10^{-12} $m^2.s^{-1}$) $D_{app(mig)}$	>50	10 to 50	5 to 10	1 to 5	<1
G	Apparent chloride diffusion coefficient (measured by a diffusion test) (10^{-12} $m^2.s^{-1}$) $D_{app(diff)}$				<5	
G	Apparent gas permeability (at $P_{upstream}$=2MPa and after drying at T=105°C) (10^{-18} m^2) K_{gas}	>1000	300 to 1000	100 to 300	10 to 100	<10
G	Liquid water permeability (at P_{max} by direct flowrate measurement, after saturation) (10^{-18} m^2) K_{liq}	>10	1 to 10	0.1 to 1	0.01 to 0.1	<0.01
	Concrete type (indicative) (European EUROCODE2 denomination)		C25 to C35	C30 to C60	C55 to C80	>C80

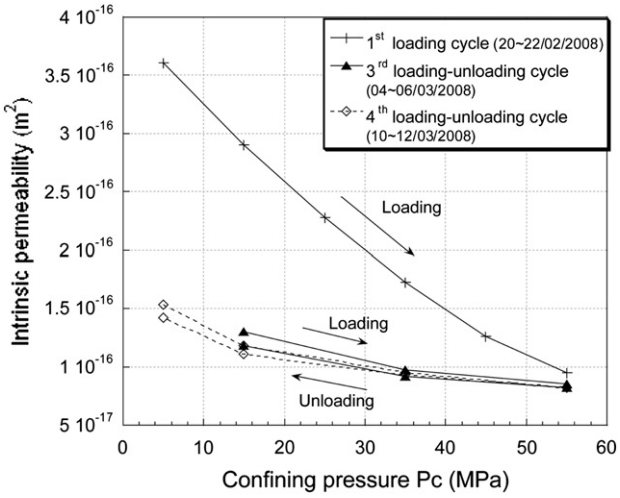

Fig. 1. Typical example of intrinsic gas permeability under confinement, obtained on a sample of mortar M1 damaged by 400 °C heat-treatment, from [11].

More precisely, during successive increases/decreases in confining pressure P_c, Fig. 1 shows the typical phases in the hydraulic behavior of a standard mortar sample, which is micro-cracked after 400 °C heat-treatment [11,12]. The first loading phase is marked by a sharp gas permeability drop (from an initial value of 3.6×10^{-16} m^2, K_{gas} is divided by 3.8 between 4 and 55 MPa confinement); this is associated to an irreversible closure of micro-cracks. Following this, the first unloading path occurs with an almost constant gas permeability (K_{gas} remains on the order of $1–1.5 \times 10^{-16}$ m^2), whereby a very limited number of micro-cracks are re-opened. The pattern of these micro-cracks (before loading) has been observed with the SEM [11]. During subsequent loading cycles, the relationship (P_c,K_{gas}) follows a non linear reversible path, so that it is no longer easy to make the difference between loading and unloading: such behavior is typical of almost intact, i.e. not micro-cracked material. Such hydraulic behavior is even more marked for initially macro-cracked materials [8,13]. On the opposite, if confining pressure has no sensitive effect upon gas permeability, it means that the porous material is intact i.e. that it does not contain micro-cracks. Therefore, a coupled investigation of gas permeability and confining pressure variations is an efficient tool to evaluate material damage, due to heat-treatment or mechanical loading. Both are used to reproduce in situ concrete aging in an accelerated manner, and at the laboratory scale.

1.3. Aims and scopes

The experimental characterization of the transport properties of UHPFRC Ductal™ has been published in [14], which has shown its excellent tightness to gas. However promising, this research related neither to the specific UHPFRC material considered in this contribution, nor to its aging behavior. Indeed, Lafarge and EDF companies need to determine whether this UHPFRC retains its durability over several tens of years, and after partial damage. These aspects are characterized experimentally herein, by performing effective gas permeability experiments (K_{gas}) under varying mechanical loading, for progressively aged concrete. Applied loading is a hydrostatic stress (or confinement P_c), obtained by placing each sample in a triaxial cell [8–11,15–17]. In order to reproduce in situ aging conditions, three progressively degrading methods are applied from an initial mature state:

(1) *partial drying* is reproduced by placing UHPFRC samples in hermetic chambers at given relative humidity (RH) until mass stabilization. $K_{gas}(P_c)$ is then characterized vs. water saturation level S_w. For comparison purposes, the reference state is chosen at mass stabilization when oven-drying at 105 °C, as in [7].

(2) UHPFRC is subjected to *diffuse damage*, as observed in situ after several tens of years seasonal thermal and hydraulic variations. This is reproduced in the laboratory by accelerated damage due to heating/cooling cycles up to 200, 300 or 400 °C. Former research on standard mortar has proven that such thermally-induced damage allows the maintenance of mechanical performance, while leading to very sensitive effects on gas permeability and on $K_{gas}(P_c)$ [15].
(3) In order to reproduce more intense degradation, UHPFRC is subjected to *localized damage*, by using a Brazilian splitting test. Tensile strain is imposed at given values along a sample diametral plane until macroscopic failure.

In cases (2) and (3), gas transport properties $K_{gas}(P_c)$ are compared to the reference state of UHPFRC, and to those of two standard cement-based materials: an ordinary concrete (OC), of composition close to that used for containment structures, and a standard mortar (M1) from our former research [10–12,15].

2. Materials and methods

2.1. Materials

A typical composition of UHPFRC-D is provided in [18]: it is made of 700–1000 kg/m^3 pure Portland cement, 200–300 kg/m^3 silica fume, 10–40 kg/m^3 super-plasticizer, 110–200 kg/m^3 water, more than 150 kg/m^3 metallic fibers, and the remaining constituents are aggregates (0–200 kg/m^3 coarse aggregates and 1000–2000 kg/m^3 fine aggregates), which maximum size ranges between as small as 0.5 and 7 mm. Its water-to-cement ratio W/C is below 0.24. The amount of super-plasticizer in UHPFRC is greater than for usual high performance concretes (HPC), in order to ensure proper workability despite the low W/C. As a matter of comparison, HPCs used by Andra for the French underground nuclear waste repository require only 10–11.5 kg/m^3 super-plasticizer per m^3 concrete [19], with a W/C of 0.39–0.43 (i.e. greater than that of UHPFRC).

The UHPFRC concrete used in this study differs from UHPFRC-D as follows: it comprises no silica fumes, and it has not been subjected to any post-hydration thermal treatment, as used on UHPFRC-D to decrease its porosity (from 6–7% to 2–3% if performed at 90 °C and 100% RH for 48 h, [20]). However, as for UHPFRC-D, its high mechanical performance is provided by an optimized Appolonian aggregate packing, with a maximum grain size of 0.6 mm, which makes it similar to a mortar, or to a micro-concrete, rather than to an ordinary concrete. Its W/C ratio is 0.23, which means that cement hydration is far from complete: this allows concrete self-repairing after limited cracking. The composition of our UHPFRC also comprises metallic fibers, which length and diameter are respectively, on average, 6 mm and 0.180 mm. More accurate data on the composition of this UHPFRC are within Lafarge™ confidential know-how, and, for that reason, cannot be reported further. Table 2 sums up the main mechanical properties of UHPFRC at 28 days air curing, as presented in [5]. It shows that, despite no thermal treatment and no pozzolanic additives, this UHPFRC has very strong mechanical performance (with 140 MPa compressive strength, 6.6 MPa tensile strength and 52GPa Young's modulus) and remarkable ductility, as evidenced by the stress sustained at 0.3 mm crack aperture (during a 3 point bending test): $\sigma_{(0.3mm)} = 2.0$ MPa.

For comparison purposes, two other cementitious materials are studied. They are respectively: (1) a standard mortar (M1), studied in [15] in order to investigate the effect of a thermal treatment (up to 400 °C) upon its mechanical and transport properties, and (2) an ordinary concrete (OC), similar to those used for containment structures of nuclear power plants.

Table 3 presents the compositions of M1 and OC. Standard mortar (M1) is mixed according to European standard EN196-1. It has a W/C ratio if 0.5, and is made with pure silica sand (from Leucate, France), which grain size distribution corresponds to European standard EN196-1, with values below 1.6 mm. Its cement is a CEM II/B-M (LL-S) 32.5R: it is composed of 69–75% clinker, 21–35% calcareous filler LL (with less than 0.2 wt.% organic matter) and 21–35% blast furnace slag S, with a fineness providing more than 10 MPa compressive strength at 2 days (and at least 32.5 MPa at 28 days maturation). When assuming a cement density of 3150 kg/m^3 [21], its paste volume is of 368 dm^3/m^3 mortar. After 6 months maturation under lime saturated water and oven-drying at 105 °C until mass stabilization, Young's modulus of M1 is of 32.5 ± 1 GPa, its compressive strength is 58 ± 0.5 MPa and its porosity (measured by the water saturation method) is of 13% ± 0.5% [15]. Mortar M1 is comparable to UHPFRC in the sense that it is composed of low-sized aggregates: the average contact surface between cement paste and aggregate is significantly lower than for OC.

Ordinary concrete (OC) complies with French standard XP18-351. It is made of pure Portland cement CEMI 52.5 PM ES, with a low C_3A content to improve resistance to sulfate attack and marine environments. Sand and bigger aggregates (of up to 20 mm diameter) are pure silica, extracted from the Palvadeau quarry (France). Its W/C ratio is 0.53: it is similar to that of mortar M1, so that it does not require the use of super-plasticizers. When assuming a cement density of 3150 kg/m^3 [21], its paste volume is of 296 dm^3/m^3 concrete, which is significantly less than mortar M1. Its porosity (measured by water saturation) is 11.5% ± 0.5%, and its compressive strength at 28 days is f_{c28} = 48 MPa. Both UHPFRC and OC have been provided to our laboratory (by Lafarge Company) as industrial pre-cast slabs, of 37 mm thickness for UHPFRC and 50 mm thickness for OC concrete.

Table 3
Composition of standard mortar M1 and ordinary concrete OC.

Constituents	Proportions (kg/m^3)
Mortar M1	
Cement CEM II/B-M (LL-S) 32.5R	450
Leucate sand (0–1.6 mm)	1350
Water (W/C = 0.5)	225
Concrete OC	
Cement CEM I 52.5 PM ES	350
Mix of sand (0–4 mm)	764
Mix of aggregates (4–20 mm)	1075
Water (W/C = 0.53)	185

Table 2
Main mechanical properties of the UHPFRC, mortar M1 and concrete OC studied.

Property	Average value for UHPFRC (without thermal treatment)	Average value for M1	Average value for OC
Uniaxial compressive strength f_{cj}	140 MPa (at 28 days)	58 +/− 0.5 MPa (after 6 months maturation under water)	48 MPa (at 28 days)
Tensile strength at 28 days f_{tj}	6.6 MPa	N/A	N/A
Tensile stress at a crack aperture of 0.3 mm (three point bending test) $\sigma_{(0.3mm)}$	2.0 MPa	N/A	N/A
Young's modulus E	52 GPa	32.5 +/− 1 GPa	N/A

2.2. Sample preparation technique

For gas permeability measurement, all samples are cut to size from mature materials. Mortar samples (of biggest aggregate diameter 1.6 mm) have been cored from a beam preserved in lime saturated water at 20 °C for 6 months. The sample size is of 37 mm diameter and 70 mm height.

UHPFRC and OC concretes are cored from the pre-cast slabs provided by Lafarge™, so that their height is imposed by the slab thickness. The UHPFRC (of biggest aggregate diameter 0.6 mm) has been air-cured for more than three months, and the OC concrete (of biggest aggregate diameter 20 mm) has been water cured for 6 months. Sample sizes are 65 mm diameter for both materials, 37 mm height for UHPFRC and 50 mm for OC concrete. As suggested by Scherer [22], the sample height should be chosen as equal to at least three times the size of the biggest aggregate, in order to ensure proper sample representativeness towards fluid transport (and to avoid preferential fluid short-cuts through paste/aggregate interfaces). It is observed that the height of OC concrete samples is 2.5 times the size of the biggest aggregate (which is close to 3 times), whereas the sample height is 62 times the size of the biggest aggregate for UHPFRC, and 44 times the size of the biggest aggregate for M1, which are both adequate according to [22].

2.3. Partial de-saturation and porosity measurement techniques

From the initial fully water-saturated state, three relative humidity (RH) levels are imposed to three different UHPFRC samples by placing each one in a different hermetic chamber at 20 °C, above a given salt-saturated solution: NaBr for RH = 59%, KCl for RH = 85% and K_2SO_4 for RH = 98%.

Water saturation level S_w represents the proportion of pores (i.e. of total porosity) filled with water. It is deduced from:

$$S_w = \frac{V_{pores}(\text{filled with water})}{V_{pores}(\text{total})} = \frac{m(RH) - m_{dry}}{m_{saturated} - m_{dry}} \quad (1)$$

where m(RH) is sample stabilized mass at given RH, m_{dry} is sample dry mass (obtained at stabilization during oven-drying at 105 °C), and $m_{saturated}$ is the initial fully water-saturated mass.

By using this so-called water saturation method, porosity $\phi_{water} = \phi$ is derived from:

$$\phi_{water} = \phi = \frac{V_{pores}(\text{total})}{V_{samples}} = \frac{m_{saturated} - m_{dry}}{\rho_{water} V_{sample}} \quad (2)$$

where ρ_{water} is water specific mass at 20 °C, V_{sample} is sample volume (measured with a caliper to an accuracy of 0.008 mm^3).

Water saturation S_w may be related to capillary pressure p_{cap} inside the porous medium. Indeed, capillary pressure p_{cap} is related to the relative humidity RH surrounding the porous medium (assumed constant) through Kelvin's law, which describes the equilibrium between air/water vapor. p_{cap} is also related to the biggest pore diameter d^i at the interface between water/air by Laplace's law. Combining these laws provides Kelvin–Laplace's equation, which allows the calculation of d^i,

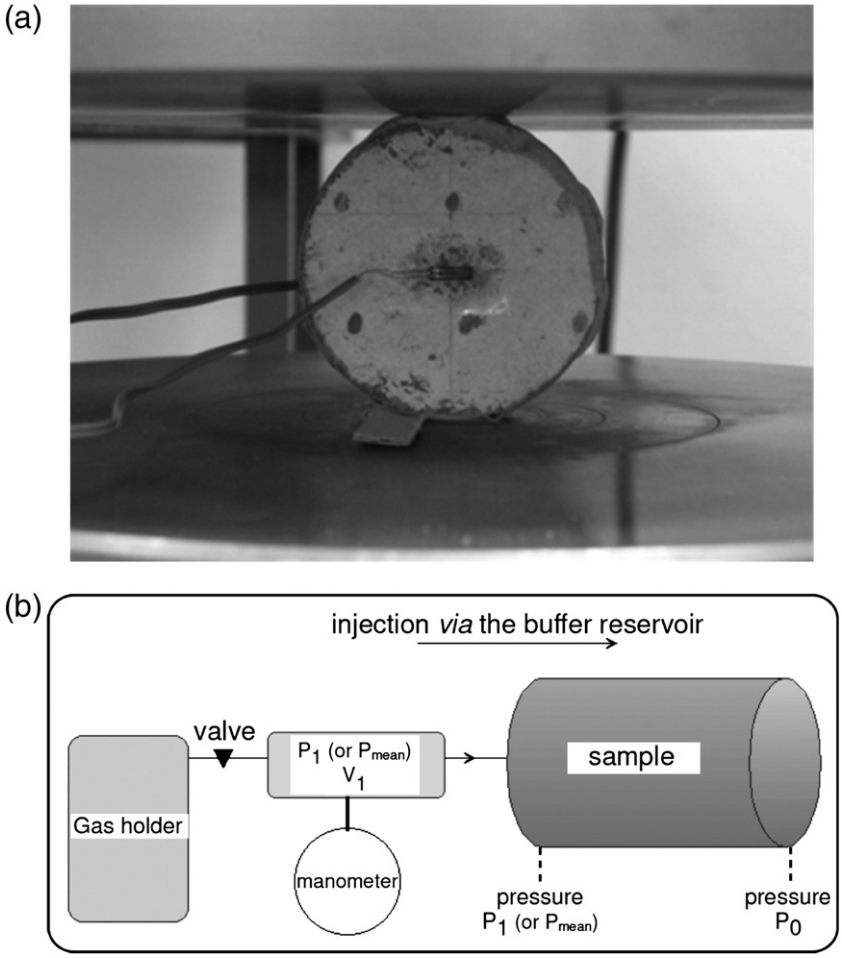

Fig. 2. (a) Macro-photograph of a UHPFRC sample used for splitting tests. The strain gage is used to impose a controlled positive strain in the middle of the end surface of the sample, in a horizontal direction. (b): Principle of the quasi-static method used for gas permeability assessment, from [8]. The sample is subjected to a fluid pressure gradient ($P_1 - P_0$) while being placed in a triaxial cell for hydrostatic stress loading.

also named smallest drained pore diameter, at given temperature T and for given RH, as:

$$d^i = -\frac{4\ \gamma_w(T)M_w}{RT\rho_{water}(T)ln(RH)} \quad (3)$$

where ρ_{water} is water specific mass (function of temperature T) [kg/m3]; R is the perfect gas constant [J/mol·K]; T is temperature [K]; M_w is water molar mass [kg/mol] and γ_w is the surface tension of water/air (also a function of temperature) [23]. In the following, all calculations are performed at 20 °C (293.15 K). From Eq. (3), at RH = 98%, the smallest drained pore diameter is calculated as $d^i = d_{saturated} = 106$ nm; at RH = 85%, it is 13 nm, which corresponds to pores between C–S–H layers (inter-layer pores); and at RH = 59%, d^i is 4 nm, which corresponds to C–S–H intra-layer pores [24,25].

Complementarily, pore size distribution and porosity ϕ_{Hg} of one UHPFRC sample (of less than 1 cm^3 volume) are assessed by Mercury Intrusion Porosimetry (MIP), with a Micromeritics™ Autopore IV 9500 apparatus, enabling intrusion pressures of up to 200 MPa. By using Laplace's law for the interface between air and mercury, this corresponds to intruded pores of diameters of 6 nm and above.

2.4. Heat-treatment procedure

Heat-treatment aims at damaging, and hence, aging, UHPFRC (and OC and M1) further than by decreasing their surrounding RH. To this purpose, heat-treatment is performed between 105 and 400 °C, which is reputed to correspond to the progressive decomposition of the C–S–H [26]. As C–S–H would also be the main concrete components to degrade due to aging, heat-treatment in such temperature range is assumed adequate to reproduce accelerated aging.

Preliminarily to heat-treatment, all samples are in so-called the reference dry state, which is obtained by oven-drying at 105 °C until mass stabilization (the RH is then less than 5%), followed by cooling down to 20 °C. The heat-treatment cycle is performed as follows: from 20 °C, samples are subjected to a heating rate of 20 °C per hour, followed by a stable phase at the target temperature T = 200, 300 or 400 °C for 1 h (for M1) or 24 h (UHPFRC and OC), and then to a cooling phase at a rate of 20 °C per hour down to 20 °C.

2.5. Brazilian splitting test

Brazilian splitting tests are performed on UHPFRC and on OC to damage them more locally than by heat-treatment, and until macro-cracking (sample failure). This also allows an evaluation of the benefit of fiber presence on gas permeability.

Preliminary to the splitting and permeability test, UHPFRC and OC samples are taken as after coring, i.e. no oven-drying is performed. Splitting is controlled up to a given value of diametral strain, which is measured by a strain gage located in the middle of one end surface of the sample, see Fig. 2(a). Table 4 indicates the different loading steps until failure.

Gas permeability is measured after each loading step, except after failure, which would require considering the sample as a small structure, and no longer as a homogeneous porous medium (despite potential localized damage).

Table 4
Evolution of splitting tests on OC and UHPFRC, during which diametral strain is imposed, and gas permeability is measured (when yes is mentionned).

Strain (10^{-6})	100	200	300	360
OC—concrete	Yes	Failure		
UHPFRC	Yes	Yes	Yes	Failure

2.6. Effective gas permeability measurement

Our gas permeability experiments consist in placing a sample of porous medium in a triaxial cell, which allows application of apply a hydrostatic stress of up to 30–35 MPa, simultaneously to a fluid** pressure gradient, see Fig. 2(b).

In its general expression for fluid transport, Darcy's law relates the fluid pressure gradient to its velocity, so that permeability is a second order tensor, which is generally admitted to be symmetrical [27] and [28]. In the following, the porous medium is assumed isotropic, and subjected to a uni-dimensional fluid flow along its axis x, so that gas permeability is reduced to a scalar quantity K_{gas} (and so are fluid pressure gradient and velocity). Gravity effects are neglected.

Usually, gas permeability K_{gas} is calculated either by the steady state method, or by the transient (pulse test) method, which choice mainly depends on the order of magnitude of K_{gas}. The steady state method is an adequate method for permeabilities $K_{gas} \geq 10^{-20}$ m^2, to avoid lengthy experimental durations. It is performed as follows.

Experimentally, fluid velocity v is assessed as the average gas volume flowrate Q_v = v/A (in m^3/s), where A is the sample cross-sectional area. As commercial flowrate-meters are not necessarily within the required measurement range, Q_v is measured by imposing a small pressure decrease ΔP (when compared to upstream pressure P_1) during time Δt [15]. This is performed by closing a valve situated upstream of a buffer reservoir, itself placed upstream of the sample, see Fig. 2(b). By assuming quasi-static flow and the perfect gas state equation, Q_v writes:

$$Q_v = \frac{V_r \Delta P}{P_{mean}\Delta t} \quad (4)$$

where V_r is the upstream buffer reservoir volume, gas pressure is P_1 on the sample upstream side, $P_0 = P_{atm}$ on its downstream side and P_{mean} is the average upstream gas pressure: $P_{mean} = P_1 - (\Delta P/2)$. Pipes volume is considered negligible when compared to V_r. In the following, P_1 = 1.5 MPa and ΔP is less than 0.1 MPa.

Along sample height L, apparent or effective gas permeability $K_{gas} = K$ is derived by expressing the pressure gradient on the sample upstream side (x = 0) through fluid mass conservation and the perfect gas state equation, so that:

$$K_{gas} = K_{int}K_{rg} = \frac{\mu Q_v\ 2LP_{mean}}{A\left(P_{mean}^2 - P_0^2\right)} \quad (5)$$

where K_{gas} is expressed in m^2, μ is gas dynamic viscosity: it is taken as $2.2x10^{-5}$ Pa.sec at 20 °C for Argon. At given saturation level S_w, K_{gas} is the product of a so-called intrinsic permeability to gas K_{int} and relative gas permeability K_{rg} [29].

2.7. Measurement of porosity (with gas) under hydrostatic loading

A dedicated test, similar in its principle to a pycnometric test, has been designed in our laboratory using gas injection inside the sample at each confinement step [12]. Gas may access the sample on one side, yet it is not allowed to flow out of it (the downstream access valve is closed). Gas is injected from a calibrated reservoir of known volume V_0 at a pressure P_1, and it is assumed perfect. After gas injection through the sample accessible pore volume, there is an equilibrium at a final pressure P_f such that, in the closed volume of the reservoir, gas pipes and sample pore volume, one gets (from the perfect gas law):

$$P_1V_0 = P_f\left(V_0 + V_t + V_p\right) \quad (6)$$

where V_p is pore volume, V_0 is reservoir volume and V_t is pipes volume. Both V_0 and V_t are determined via a preliminary test (which consists in replacing the sample by a non porous one). From pore volume V_p data, conventional porosity (measured with gas) is calculated by using the

Table 5
Porosity ϕ_{water} and water saturation level S_w, measured for three different UHPFRC samples placed respectively at 59, 85 and 98% RH. $d_{saturated}$ is the biggest water-saturated pore diameter according to Kelvin–Laplace's law used at 20 °C [23].

UHPFRC Sample	Dry mass after 105 °C oven-drying (g)	Saturated mass (g)	Porosity ϕ_{water} (water saturation method) (%)	Imposed RH (%)	$d_{saturated}$ (nm)	Stable mass at given RH (g)	Water saturation S_w at stabilization at given RH
F	295.2	307.99	10.4%	59	4	304.68	**74%**
G	293.65	305.74	**9%**	85	13	303.12	**78%**
H	294.48	305.88	**9%**	98	106	305.27	**95%**

initial sample volume V_{sample}, as: $\phi_{gas}(P_c) = V_p/V_{sample}$ at each value of confinement P_c.

3. Results and discussion

3.1. Effect of partial drying upon gas permeability $K_{gas}(P_c)$

Table 5 sums up the mains results for porosity ϕ_{water} and saturation level S_w at given RH, for UHPFRC alone.

3.1.1. Pore volume

Porosity ϕ_{water} is on average 9.5% +/− 0.5, which is, as expected, significantly greater than porosity ϕ_{Hg} given by MIP at a value of 6.4%. According to [7], such porosity level for ϕ_{water} corresponds to the range of high durability concrete (not "very high durability"), and expected dry gas permeability (after 105 °C oven-drying and at P_{gas} = 2 MPa) should be within 10^{-17}–10^{-16} m^2. Fig. 3 shows that for our UHPFRC, dry gas permeability is hardly affected by confining pressure changes, and that it ranges between 0.92 and $1.5x10^{-18}$ m^2. Such gas permeability classifies our UHPFRC as of very high durability (and not of high durability only), as suggested by porosity values alone. This justifies the use of gas permeability, as a more accurate indicator of concrete durability than porosity.

3.1.2. Partial drying and pore size distribution

At mass stabilization at given RH (from the initially fully water-saturated state, i.e. during a first desorption), water saturation level S_w is 95% at RH = 98% (sample H), whereas S_w = 78% at RH = 85% (sample G), and it decreases down to 74% only at RH = 59% (sample F). Although these tests were performed on different samples (which is bound to affect the results), we observe that only 4% variation in S_w occurs between RH = 85 and 59%. When applying Laplace's law at 20 °C, this corresponds to the drying of pores of diameters between 13 and 4 nm, which are, for the former, C–S–H inter-layer pores, and for the latter, C–S–H intra-layer pores: according to Kelvin–Laplace's law, between 85 and 59%RH, all pores bigger than those within the C–S–H layers are emptied. Our measurements show that only 4% of the total porosity of our UHPFRC (i.e. S_w(RH = 85%) − S_w(RH = 59%)) is made of pores in the range [4,13]nm. Similarly, only 5% of the UHPFRC porosity is made of pores bigger than 106 nm (which dry at RH = 98%), and 22% of the porosity is composed of pores bigger than 13 nm. Most of the porosity (i.e. 74% of it) is below 4 nm, i.e. it is within the C–S–H layers. This is a consequence of the optimization of the UHPFRC microstructure, which provides very thin pore sizes, and, hence, excellent resistance to fluid ingress.

As a matter of comparison, MIP results for pore size distribution of reference dry UHPFRC are given in Fig. 4. Down to 6 nm (lower limit of MIP), UHPFRC pore size distribution is unimodal, with a pore peak at 12 nm diameter, followed by a sharp decrease in pore diameters bigger than this value. The small difference in water saturation between RH = 85% (13 nm of biggest saturated pore diameter) and RH = 59% (4 nm of biggest saturated pore diameter) is justified by MIP, as this range of diameters lies in the domain of the sharp decrease in pore volume. Except for a small peak at 3.85 μm, there are no more pores, which diameter is larger than 100 nm. Pores bigger than 80 μm are attributed to micro-cracks, created by sample cutting, to fit inside the MIP device: they are not predicted by Kelvin–Laplace's law as capillary pores present at 98%RH or below. Moreover, no pores smaller than 6 nm are accounted for by MIP, so that the main pore diameter for UHPFRC should be of 12 nm. This is not consistent with our saturation level measurements, see Table 5 again: S_w remains at 74% after pores bigger than 4 nm are dried, according to Kelvin–Laplace's law.

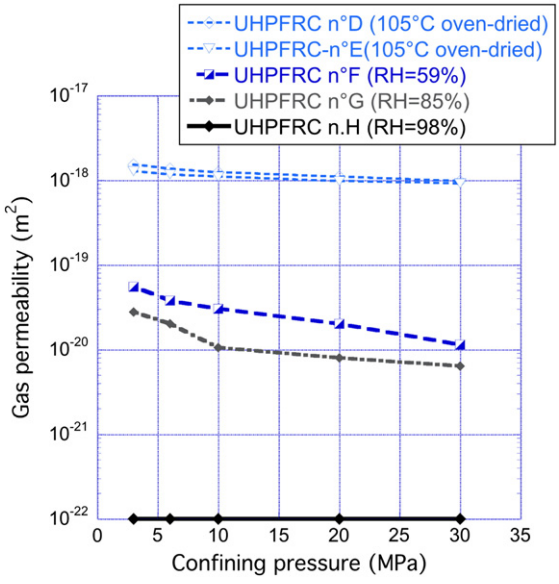

Fig. 3. Apparent gas permeability of partially-dried UHPFRC under increasing confining pressure—comparison with the initial dry reference state.

3.1.3. Gas permeability in the partially water-saturated state

While providing a few points of the desorption (RH,S_w) curve, our aim is to observe whether the UHPFRC may exhibit a hydraulic cut-off, whereby gas cannot flow through the medium at given confinement level, while it is not fully saturated. Therefore, in the following, apparent gas permeability K_{gas} of UHPFRC is provided (1) after mass stabilization at given RH, and (2) after oven-drying at 105 °C, both under confinements up to 30 MPa, see Fig. 3. Sample H is saturated by 95%: it has a gas permeability lower than 10^{-22} m^2, and no actual gas passage was measured on the sample downstream side, when applying a fixed gas pressure on the upstream side for more than 4 h. It is concluded that a gas permeability equal to zero corresponds to S_w = 95% (RH = 98%). By using Laplace's law at RH = 98% and 20 °C, this means that there is no continuous path in UHPFRC composed of pores, which diameter is bigger than 106 nm.

For samples F and G, which are saturated below S_w = 95%, gas permeability decreases with increasing confinement, and it is recorded at very low values, ranging from 10^{-20} m^2 to $7x10^{-20}$ m^2 (sample F, S_w = 74%) or $8x10^{-21}$ m^2 to $2x10^{-20}$ m^2 (sample G, S_w = 78%), see Fig. 3 again. As expected, more saturated sample G (S_w = 78%) has consistently lower gas permeability than sample F (S_w = 74%). For both these samples at a confining pressure P_c = 30 MPa, K_{gas} is between 10^{-20} m^2 and $8x10^{-21}$ m^2, which is considered as an actual hydraulic cut-off. Indeed, for $K_{gas} = 10^{-20}$ m^2 (respectively $K_{gas} = 8x10^{-21}$ m^2),

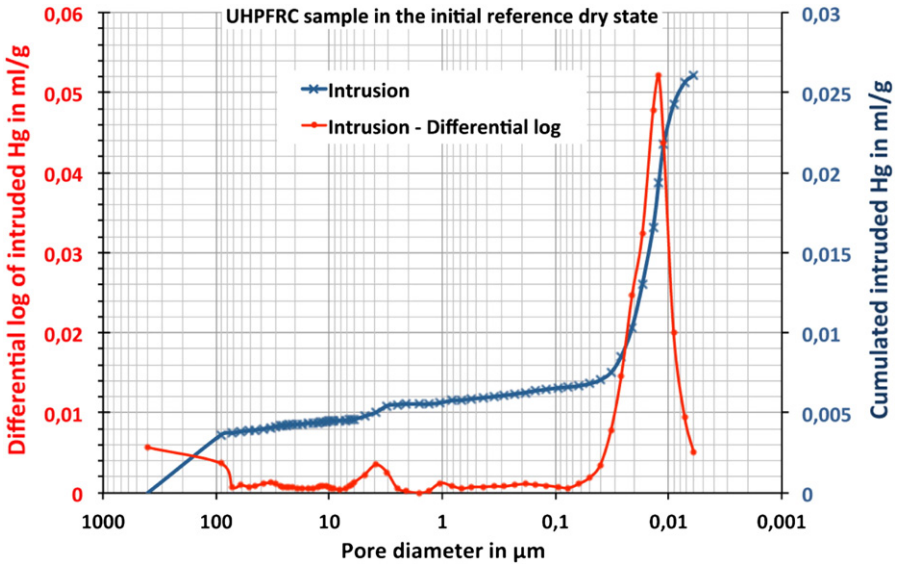

Fig. 4. Mercury intrusion porosimetry test on UHPFRC in the initial reference dry state—mercury pressures are applied up to 200 MPa.

at 0.2 MPa gas pressure gradient (which is on the order of that imposed in situ), gas flowrate is of only 8.14 µl/h (respectively 6.51 µl/h); at an upper limit of 0.5 MPa gas pressure gradient, gas flowrate is of 26 µl/h (respectively 20.8 µl/h).

3.2. Assessment of a dry reference state for $K_{gas}(P_c)$

We aim to compare the effect of gradual damage upon concrete durability, as measured by gas permeability, in relation to a reference state. It is chosen as the dry state at 105 °C, associated to a hydrostatic loading P_c up to 30 MPa or 25 MPa (for mortar M1). Fig. 5 shows the evolution of K_{gas} with P_c, for the three materials (UHPFRC, OC and M1), when all are in the reference state. A log scale is used, as it is more adapted to the high permeability contrasts measured.

One observes that UHPFRC is significantly less permeable than OC and mortar M1, with values ranging between 0.92 and $1.5x10^{-18}$ m^2 (see also previous Sub-section 3.1.) depending on P_c, whereas these range between 6.0 and $6.5x10^{-18}$ m^2 for M1, and between 20.1 and $49x10^{-18}$ m^2 for OC. However, reference dry gas permeability values for UHPFRC remain comparable with former results obtained in our lab [17] on several high performance concretes, which gas permeability is of ca. 5^{*} 10^{-18} m^2 (and 6 to 8% porosity). Reference dry gas permeability for UHPFRC is quite low, but not exceptional. Moreover, contrarily to UHPFRC and OC, mortar M1 is almost insensitive to confining pressure increase: this is attributed to the fact that no significant micro-cracking has occurred during its drying.

Normalized gas permeability is more adapted to evaluate the material sensitivity to confining pressure, which relates directly to its damage level: we use the ratio between gas permeability at given P_c and that at the lowest P_c used, i.e. K(Pc)/K(Pc = 3 MPa), see Fig. 6. This allows to clear out the initial gas permeability K(Pc = 3 MPa), which order of magnitude differs significantly from one material to the other, see Table 6: K(Pc = 3 MPa) is on average $1.4x10^{-18}$ m^2 for 105 °C oven-dried UHPFRC, while it represents 4.6 times this value for M1, and 35 times this value for OC.

Two different phases are observed. The first one is the first loading phase, during which OC concrete is the most sensitive to P_c increase with 60% reduction in gas permeability at P_c = 30 MPa. This means

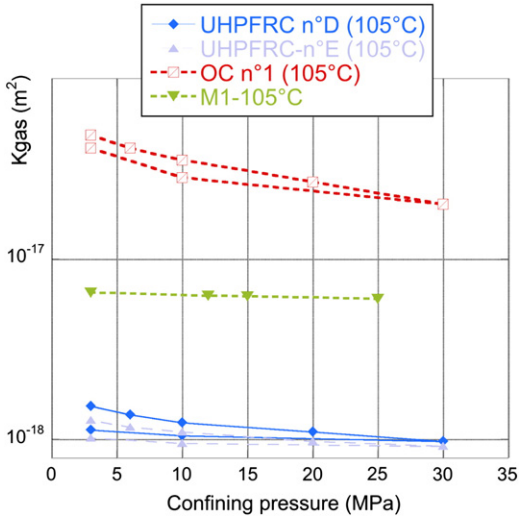

Fig. 5. Gas permeability vs. confining pressure in the initial dry reference state, i.e. after 105 °C drying until mass stabilization, for UHPFRC, OC and M1.

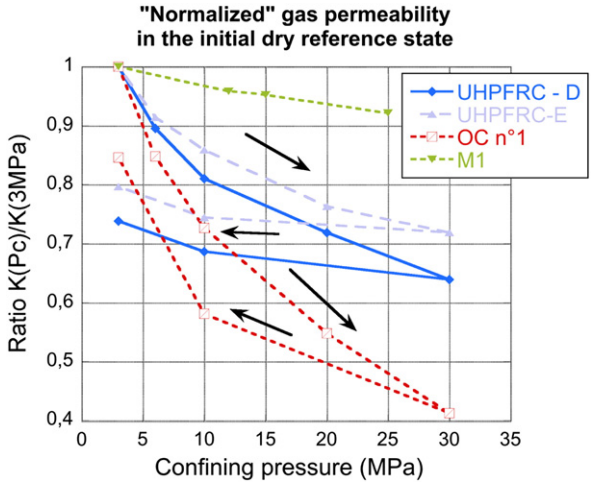

Fig. 6. Influence of confining pressure on the relative permeability ratio K(Pc)/K(3 MPa) in the initial dry reference state, for UHPFRC, OC and M1.

Table 6
Increase in gas permeability for the three materials heat-treated at 400 °C, at a fixed confining pressure P_c = 3 MPa. The initial gas permeability is obtained after oven-drying at 105 °C until mass stabilization.

Material	Average initial gas permeability K (10^{-18} m^2)	K(material)/K(UHPFRC)	Permeability after 400 °C heat-treatment (10^{-18} m^2)	K(material)/K(UHPFRC) after 400 °C heat-treatment
UHPFRC	1.4	**1**	12	**1**
Mortar	6.5	**4.6**	239	**20**
Ordinary concrete	48.7	**35**	641	**53**

that OC is initially micro-cracked. As already noted from Fig. 5, mortar M1 is almost insensitive to P_c, which means that this material has not been significantly affected (wrt. its gas transport ability) by 105 °C heating. As OC, UHPFRC is sensitive to confinement, with around 30% reduction in gas permeability at Pc = 30 MPa. During the unloading phase, the behavior of OC concrete is less hysteretic than that of UHPFRC: the difference with K_{gas} during the first loading phase is smaller for OC than for UHPFRC. This observation means that, when unconfined, the gas passages within the UHPFRC re-open less than those of the OC concrete. These gas passages within UHPFRC are certainly not micro-cracks, as its optimized composition allows us to infer.

Fig. 7(a) shows a typical SEM image of UHPFRC microstructure in the dry reference state. At the observation scales allowed by the SEM (down to several hundreds of nm), no micro-cracks have been observed. However, our UHPFRC has not been subjected to heat-treatment, which would allow for improving the contact between fibers and paste [5].

From SEM observations of UHPFRC and M1 [12] in the dry reference state, it is inferred that the amplitude of K_{gas}, and its sensitivity to confining pressure variations, are due to both (1) the bonding strength between cement paste and metallic fiber (and/or cement paste and sand aggregate), and to (2) the fineness of the microstructure (sand grains are of less than 0.6 mm diameter for FUHPC and 1.6 mm for M1). Both bonding strength and fineness of microstructure have been optimized for UHPFRC, when compared to M1 (and OC). This has direct consequences on fluid transport properties: when comparing UHPFRC to M1 and OC, K_{gas} is significantly lowered, as is its sensitivity to confining pressure changes, see Figs. 5 and 6.

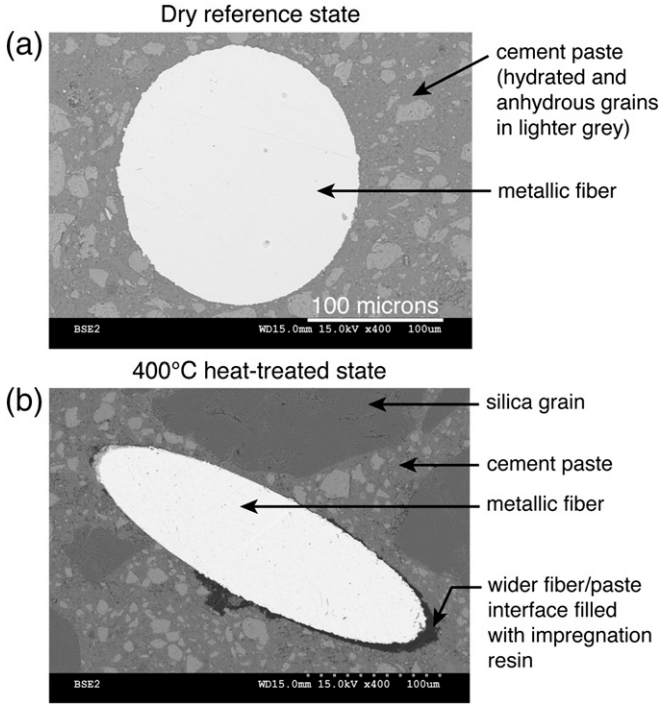

Fig. 7. SEM observations of the fiber–matrix interface (BSE detector). (a): Image of UHPFRC in the initial reference state; (b): this photograph is typical of 400 °C heat-treated UHPFRC.

3.3. Effect of diffuse damage upon durability

3.3.1. Microstructure changes

Diffuse damage after heat-treatment is visualized by SEM imaging, see Fig. 7(a) and (b) for UHPFRC, and reference [12] for mortar M1. For UHPFRC, it is observed that the main damage feature due to heat-treatment at 400 °C is a degradation of the interface between fiber and cement paste, as the presence of impregnation resin (in dark) shows. However, this interfacial opening is not observed on all fibers, and none are degraded along all of their surface: there is a limited debonding between fiber and cement paste.

For mortar M1, the degradation after 400 °C heat-treatment is more extensive, with (1) pore widening (observed by MIP) and (2) heat-induced micro-cracks present both at the interface between sand aggregates and cement paste, and within the cement paste, which links two neighboring aggregate/paste interfaces [15]. Pore widening is associated to C–S–H decomposition in the 105–400 °C range, and micro-cracking is attributed to the differential dilation between cement paste and aggregates. For OC, similar damage mechanisms are inferred. However, for UHPFRC, no micro-cracking similar to that of M1 is observed. Indeed, the design of UHPFRC comprises a very limited ITZ (Interface Transition Area), and a limitation in the rigidity difference between aggregates and paste (owing to an increase in cement paste rigidity, and to its greater proportion wrt. sand) [5]. These are bound to help limit the occurrence and extent of micro-cracks. Moreover, C–S–H decomposition is hindered by the difficulty to access the bulk of the samples, owing to very fine pore sizes.

3.3.2. Gas permeability $K_{gas}(P_c)$ after diffuse damage

After heat-treatment, gas permeability changes are represented 1) as a function of heat-treatment temperature T (for a given low confinement value of 3 MPa), see Fig. 8, then 2), as a function of confining pressure, see Figs. 9, and 3) normalized by reference gas permeability K_{gas}(T,Pc)/K_{gas}(105 °C,Pc). Each different representation enhances a specific feature of gas permeability changes with heat-treatment and confinement, and compares the three materials (UHPFRC, OC and M1).

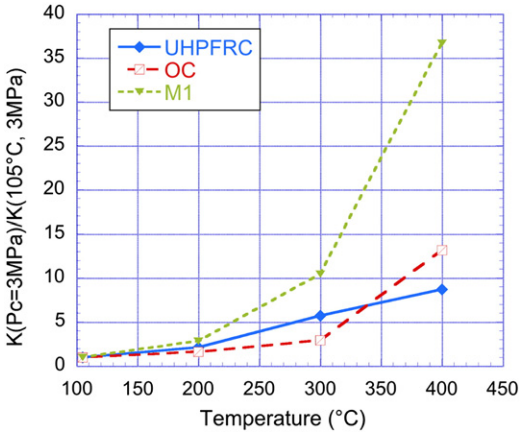

Fig. 8. Effect of heat-treatment upon gas transport—gas permeability ratio K(Pc = 3 MPa, T)/K(Pc = 3 MPa, 105 °C) vs. heat-treatment temperature T for UHPFRC, OC and M1.

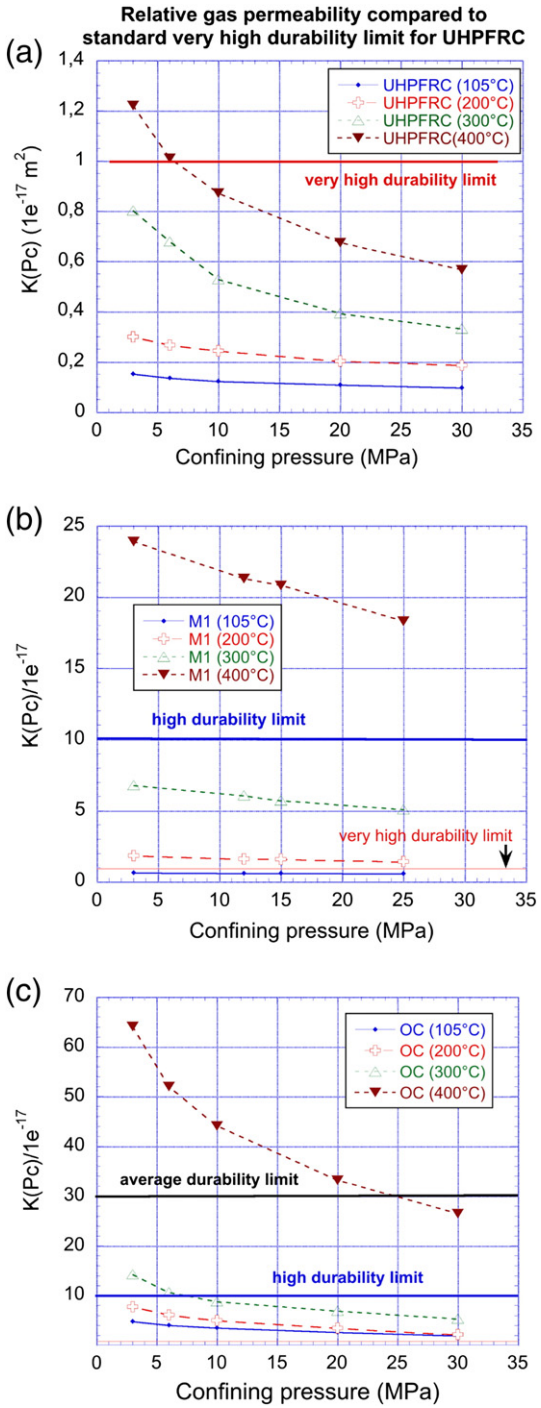

Fig. 9. Effect of heat-treatment upon gas transport—normalized gas permeability $K(Pc)/10^{-17}$ for (a) UHPFRC, (b): M1, (c): OC at different heat-treatment temperatures and confinement.

3.3.2.1. Effect of heat-treatment at low confinement. In Fig. 8, for each material individually, gas permeability variations are normalized i.e. compared to the K_{gas} value in the dry reference state at a low $P_c = 3$ MPa. By using such representation, we amplify the effect of heat-treatment alone upon K_{gas}, when compared to that at greater confinement P_c.

Fig. 8 indicates that heat-treatment induces an increase in $K = K_{gas}(Pc = 3\ MPa)$, so that it is multiplied by 1.6 (for OC), 2.1 (for UHPFRC) and 2.8 (for M1) at T = 200 °C. A greater increase in $K = K_{gas}(Pc = 3\ MPa)$ is measured at T = 300 °C: it is multiplied by 2.9 for OC, 5.7 for UHPFRC and 10.4 for M1. A significantly greater increase is measured at 400 °C, with a multiplication of $K = K_{gas}(Pc = 3\ MPa)$ by 8.7 for UHPFRC, 13.2 for OC and 36.7 for M1. Therefore, UHPFRC sustains the smallest increase in the range T = [200; 400]°C, whereas the greatest damage due to heat-treatment is sustained by mortar M1. OC sustains the smallest damage up to 300 °C, whereas its damage after 400 °C heat-treatment is greater than for UHPFRC.

For M1 and OC, the main damage features are related to pore widening and micro-cracking, see Sub-section 3.3.1. Also, M1 is made of a composed cement, which comprises not only clinker, but also limestone filler and blast furnace slag. Due to these additions, the stoichiometry of C–S–H in M1 is wider than for OC, which uses clinker only as a cement [30]. Therefore, the decomposition of C–S–H in mortar M1 is bound to occur within a greater temperature range than for OC, as it corresponds to a wider range of chemical reactions than for OC. Besides the fact that mortar M1 contains a greater proportion of cement paste than OC (368 dm^3/m^3 vs. 296 dm^3/m^3), this wider C–S–H stoichiometry is interpreted as the main reason for the earlier and greater increase in $K_{gas}(Pc = 3\ MPa)$ of mortar M1 with increasing T, when compared to OC. On the opposite, UHPFRC remains sound and scarcely damaged when compared to M1 and OC, with very few changes in its pore geometry, see Sub-section 3.3.1., so that its permeability is much less degraded than that of OC and M1.

Complementarily, Table 6 shows that at low confinement ($P_c = 3$ MPa), OC concrete has the highest gas permeability of all three materials, either before or after heat-treatment at 400 °C. When compared to UHPFRC in the reference dry state, mortar M1 has a greater K_{gas} by 4.6 times only, whereas OC has a 35 times greater K_{gas}. After 400 °C heat-treatment, OC still has the greatest ratio K(material)/K(UHPFRC), with a value of 53, whereas M1 displays a value of 20.

However, the most degraded material (from its own dry reference state) is M1, see Fig. 8 again. It is interpreted that OC, being initially more permeable, is less sensitive to damage by heat-treatment: to occur, gas passage through OC does not rely so much on pore widening or micro-cracking as M1 does.

3.3.2.2. Durability assessment after heat-treatment. Fig. 9 displays absolute gas permeability values, through the ratio $K(Pc)/10^{-17}\ m^2$ vs. confining pressure for each heat-treatment temperature T = 200, 300 and 400 °C, and compared to the reference dry state, for (a): UHPFRC, (b): M1 and (c): OC. The gas permeability value of $10^{-17}\ m^2$ corresponds to the "very high durability limit" (it is indicated by a red line in Fig. 9), while $10^{-16}\ m^2$ is the "high durability limit" (blue line) and $3x10^{-16}\ m^2$ is the so-called "average durability limit" (black line). Vertical scale increases from UHPFRC (0–1.4) to OC (0–70), in order to enhance the evolution of $K(Pc)/10^{-17}\ m^2$ for each material.

It is observed that UHPFRC has a very progressively increasing permeability K_{gas} with increasing heat-treatment temperature, whatever the confinement applied. Except at $P_c = 3$ and 6 MPa after 400 °C heat-treatment, K_{gas} remains below the very high durability limit, which testifies of the excellent behavior of UHPFRC after diffuse damage.

On the opposite, mortar M1 remains below the very high durability limit only after 105 °C oven-drying; it is within the high durability materials after 200 and 300 °C heat-treatment, and below the average durability limit after 400 °C heat-treatment. Of all three materials investigated, OC concrete is the least resistant to damage by heat-treatment: even after 105 °C oven-drying, it is above the very high durability limit; it is below the high durability limit up to T = 300 °C and $P_c \geq 6$ MPa. Otherwise, it is above the average durability limit (T = 400 °C and $Pc \leq 25$ MPa). For both M1 and OC, the high durability behavior is preserved up to 300 °C (and $P_c \geq 6$ MPa), which is the threshold above which gas starts to pass at a more significant flowrate (with $K_{gas} \geq 3x10^{-16}\ m^2$).

3.3.2.3. Sensitivity of heat-treated concretes to confining pressure variations. The sensitivity to P_c changes is represented in Fig. 10, by the ratio K(T,Pc)/K(105 °C,Pc) vs. confining pressure for (a): UHPFRC, (b): mortar M1, and (c): OC, for the different temperatures T = 200, 300 and 400 °C, and in the dry reference state: in this case, the ratio is equal to one, whatever

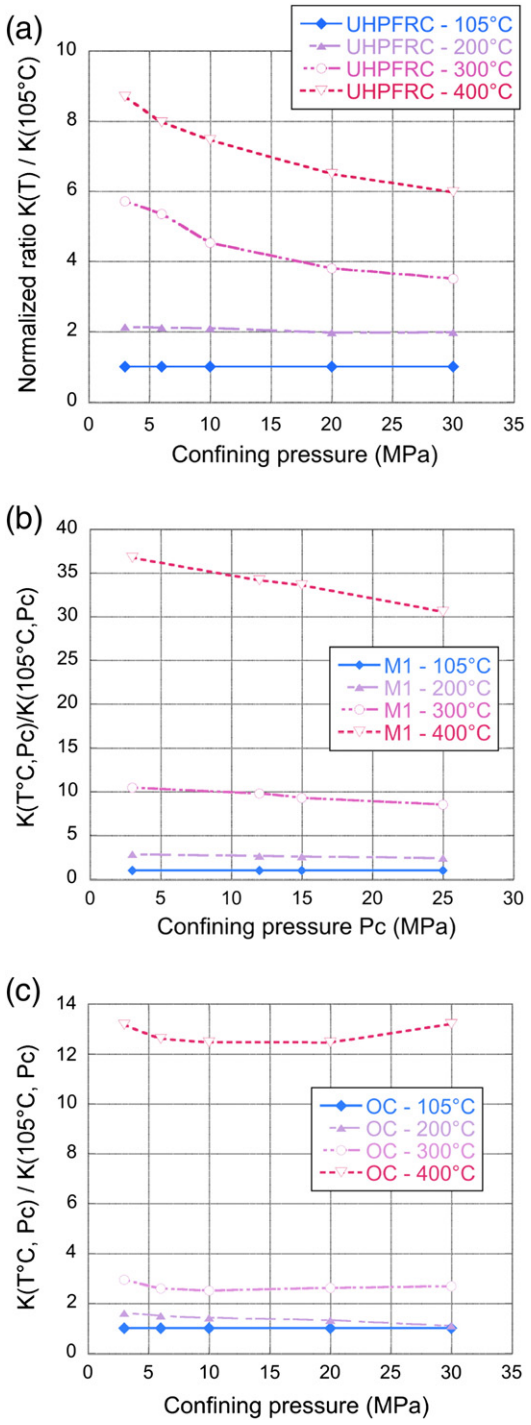

Fig. 10. Effect of heat-treatment upon gas permeability ratio K(T°C, Pc)/K(105 °C, Pc) for (a): UHPFRC, (b): M1 and (c): OC.

P_c. Such representation is useful, as the effect of initial confinement is taken into account by the normalization operation, so as to analyze the sole effect of confinement due to heat-treatment above 105 °C.

For UHPFRC, the sensitivity to confining pressure is almost constant after 200 °C heat-treatment, with K(T,Pc)/K(105 °C,Pc) varying in the narrow range 1.9–2.1 whatever Pc, see Fig. 10(a). This value represents twice that after 105 °C oven-drying: it is attributed to the creation of gas passages, which do not close significantly up to Pc = 30 MPa. This is usually observed for a network of small width passages (below 1Âμm). After 300 °C and 400 °C heat-treatment, normalized gas permeability at low confinement K(T,Pc = 3 MPa)/K(105 °C,Pc =3 MPa) is greater than after 105 °C or 200 °C heat-treatment, with values of 5.7 at T = 300 °C and 8.7 at T = 400 °C: this testifies of a greater created volume of gas passages with increasing T, as already observed from Fig. 8. However, contrarily to 200 °C heat-treatment, the ratio K(T,Pc)/K(105 °C,Pc) reduces progressively with increasing confinement, with values ranging from 3.5 to 5.7 at T = 300 °C, and 5.9–8.7 at T = 400 °C, for P_c = 3–30 MPa. From these observations, it is interpreted that a proportion of created gas passages is wide enough to close when Pc increases. SEM observations after 400 °C heat-treatment show that passages as wide as several microns to several tens of microns exist, which justify this interpretation, see Fig. 7(b) again. Since gas passages created by heat-treatment are included in a low permeability matrix, their closure due to confinement has a greater amplitude than for M1 and OC, see also Fig. 10(b) and (c). Besides, for T > 200 °C, the ratio K(T,Pc)/K(105 °C,Pc) follows a similar slope whatever P_c: the progressive closure of gas passages occurs in a parallel manner. It is interpreted that cracks created after 400 °C heat-treatment, which close above P_c = 10 MPa, have a similar initial opening as those created at T = 300 °C. They are, however, more numerous after 400 °C heat-treatment.

Fig. 10(b) and (c) represent the ratio K(T,Pc)/K(105 °C,Pc) for mortar M1 and OC concrete. As for UHPFRC, for P_c ranging from 3 to 30 MPa, mortar M1 exhibits a temperature threshold between 200 and 300 °C, from which the permeability ratio increases significantly, up to 8.5–10.4 (for T = 300 °C) or 30.5–36.7 (for T = 400 °C), whereas it remains in the range 2.4–2.8 at T = 200 °C. For OC, the threshold above which K(T,Pc)/K(105 °C,Pc) increases significantly is rather at T ≥ 300 °C: at T = 200 °C, K(T,Pc)/K(105 °C,Pc) varies in the range 1.1–1.6, whereas it is within 2.5–2.9 at T = 300 °C and within 11.1–13.2 for T = 400 °C.

3.3.3. Porosity changes $\phi_{gas}(P_c)$ (measured with gas) after diffuse damage

Complementarily to gas permeability, this experiment provides a *direct* assessment of porosity changes under increasing P_c for dry reference and heat-treated materials (OC and UHPFRC only), see Table 7.

First, one observes no obvious relationship between $\phi_{gas}(P_c)$ and gas permeability K_{gas}, whereby a greater $\phi_{gas}(P_c)$ would be associated to greater K_{gas}. In particular, in the dry reference state and at low confinement P_c = 2 MPa, porosity $\phi_{gas}(P_c)$ is higher for UHPFRC (with a value of 9.1%) than for OC ($\phi_{gas}(P_c = 2\ MPa) = 8.4\%$); in the meantime, at a close P_c = 3 MPa, the average gas permeability of OC is 35 times that of UHPFRC, see Table 6. This means that the size of gas pathways (expected to be smaller for UHPFRC) and their tortuosity are predominant over their volume (as measured by $\phi_{gas}(P_c)$).

After 400 °C heat-treatment, OC undergoes an absolute increase by 1.5% in porosity $\phi_{gas}(P_c)$, and UHPFRC an increase by 3.1%, see Table 7. Despite a greater increase in porosity $\phi_{gas}(P_c)$ for UHPFRC than for OC, the gas permeability of UHPFRC remains very low, with an average value of $12x10^{-18}$ m^2, whereas the gas permeability of OC becomes 53 times that of UHPFRC, see Table 6 again.

We interpret these results as the signature of different degradation modes due to heat-treatment: for OC (assumed similar to M1), damage is rather associated to pore widening and cement paste (and paste/aggregate) micro-cracking; for UHPFRC, damage is limited to partial fiber/paste de-bonding. The greater increase in $\phi_{gas}(P_c)$ for UHPFRC (than for OC) is attributed to a greater volume of damage of the former. However, fiber/paste de-bonding does not connect significantly through to the cement paste volume, so that its effect on K_{gas} is more limited than the damage (pore widening and extensive micro-cracking) sustained by OC.

Our results, which show greater porosity $\phi_{gas}(P_c)$ associated to lower gas permeability increase for UHPFRC than OC, mean that pore widening and micro-cracking have a greater effect upon gas permeability than fiber/paste de-bonding.

However, as expected, for both materials, porosity $\phi_{gas}(P_c)$ decreases progressively with increasing confining pressure. As for mortar M1 [12], this is evidence that an increase in P_c induces a closure of gas passages

Table 7
Porosity under loading $\phi_{gas}(P_c)$, measured with gas under different confining pressures P_c: comparison between OC and UHPFRC.

Sample	OC (dry reference state)			OC (400 °C)			UHPFRC (dry reference state)			UHPFRC (400 °C)		
Confining pressure (MPa)	2	20	30	2	20	30	2	20	30	2	20	30
Porosity under loading $\phi_{gas}(P_c)$ (%)	8.4	N/A	N/A	9.9	9.4	9.3	9.1	8.7	8.44	12.2	11.6	11.44

inside the solid matrix. After 400 °C heat-treatment, this decrease is very close for UHPFRC and OC: for an increase in P_c from 2 to 30 MPa, it represents $(0.6/9.9) = 6.1\%$ for OC and $(0.76/12.2) = 6.2\%$ for UHPFRC. This is unexpected, as OC has a smaller sensitivity to confinement changes than UHPFRC, see Fig. 10(a) and (c). Again, this result is associated to the size and tortuosity of gas pathways, which are of a very different nature for UHPFRC and OC. Gas pathways in UHPFRC, created by the heat-treatment, are more easily closed by confinement than for OC.

3.4. Effect of localized damage upon gas permeability $K_{gas}(P_c)$

The splitting test progressively induces a localized material cracking until tensile failure, which is located in a diametral plane of the initially circular cylindrical sample. For UHPFRC, failure is obtained at a maximum tensile strain of 360 μm/m, with a residual crack aperture of 280 μm, see Fig. 11(a) and (b). For OC, tensile failure occurs much earlier than for UHPFRC, at a maximum strain value between 100 and 150 μm/m. As expected, the presence of short metallic fibers enhances considerably the ductility of UHPFRC [31].

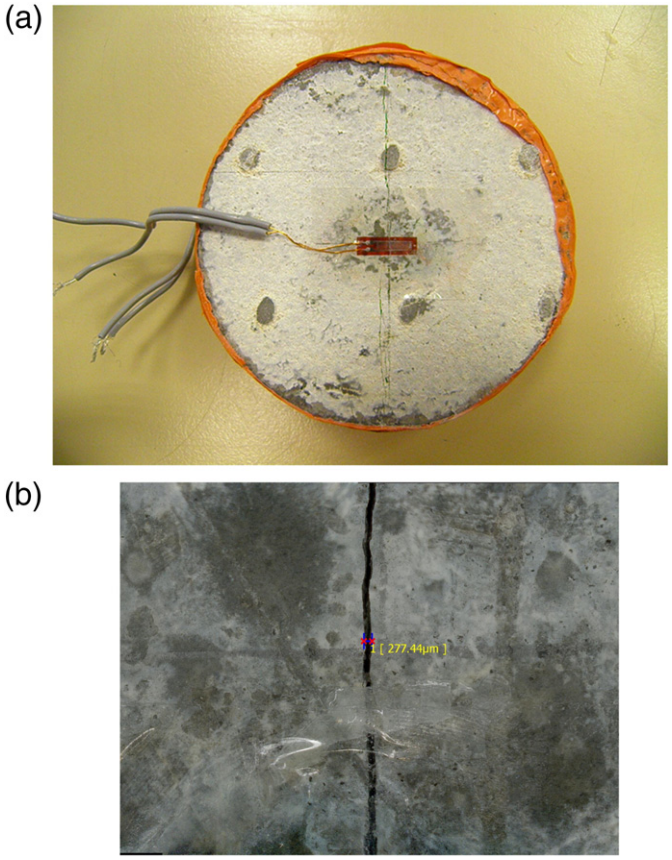

Fig. 11. (a) Macro-photograph of the failed UHPFRC sample at 360 micro strains (from gage strain measurements) and (b): corresponding crack aperture of the failed UHPFRC sample, measured after unloading at an average value of 280 μm by using a 3D optical microscope.

For UHPFRC subjected to splitting, associated gas permeability results are plotted in Fig. 12. Initially, the sample is partially water-saturated, with a saturation level S_w ranging between 80 and 95%. Complementarily to previous heat-induced damage, this aims at reproducing a sudden accidental failure, prior to full concrete drying. The initial saturation explains that lower gas permeabilities are measured than in the dry reference state: these are on orders of magnitude of 10^{-20}–10^{-21} m^2, rather than on the order of 10^{-18} m^2 in the dry reference state.

In Fig. 12, we observe a significant, yet limited, increase in gas permeability due to the splitting test: at low confinement $P_c = 3$ MPa, K_{gas} increases from an initial $4.5x10^{-21}$ m^2 to $1.0x10^{-20}$ m^2 at 300 μm/m, i.e. by 2.2 times; at the maximum confinement $P_c = 30$ MPa, K_{gas} increases from an initial $4.1x10^{-21}$ m^2 to $6.3x10^{-21}$ m^2 at 300 μm/m, i.e. by 1.5 times. This means that until as high a strain as 300 μm/m, the test has created micro-cracking only. Indeed, a macro-crack would have induced a significantly stronger increase in gas permeability [13]: for CEMI or CEMV-based HPC samples, which are initially macro-cracked by a Brazilian splitting test (as here), gas permeability ranges between 0.9 and $32x10^{-15}$ m^2, whereas 105 °C oven-dried gas permeability is on the order of 10^{-18} m^2 (i.e. 2 to 3 orders of magnitude lower) [24]. Moreover, for UHPFRC, the decrease in gas permeability with increasing P_c occurs mainly between 3 and 5 MPa: it then remains virtually insensitive to higher P_c increase, up to 30 MPa. This indicates that most of the micro-cracks created by splitting are closed by a small increase in P_c, from 3 to 5 MPa only. It is concluded that UHPFRC has an excellent resistance to progressive micro-cracking, by retaining its low gas transport ability up to more than 300 μm/m tensile strain.

As a matter of comparison, an OC sample has been subjected to splitting. Gas permeability results are plotted only up to 100 μm/m, since its failure has occurred soon after this value (i.e. below 150 μm/m), see Fig. 13. As for UHPFRC, the OC sample used in this experiment is partially water-saturated, by more than 80%.

The increase in gas permeability is significant at $P_c = 1$ MPa, with an initial value of $8x10^{-18}$ m^2 and a value of $15.5x10^{-18}$ m^2 at 100 μm/m: micro-cracks created by splitting induce a significantly greater K_{gas} (greater by 1.9 times). Moreover, contrarily to UHPFRC, whatever the

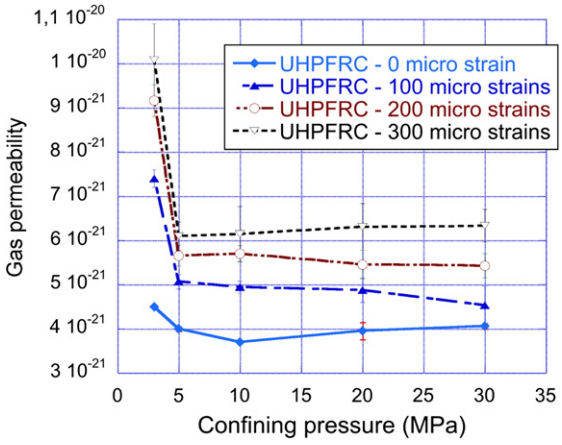

Fig. 12. Effect of tensile strains induced by a splitting test on UHPFRC gas permeability. Tests were performed on the same sample, which is initially partially water-saturated.

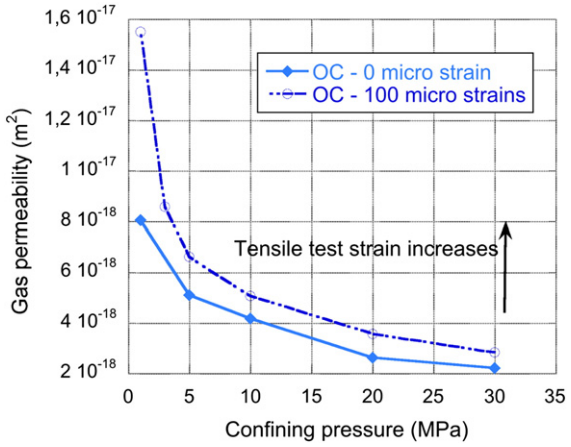

Fig. 13. Increase in gas permeability due to tensile stress for OC. The influence of confining pressure, revealing the closure of cracks, is without ambiguity.

tensile strain sustained, OC is sensitive to P_c increase: when P_c increases from 1 to 30 MPa, K_{gas} is divided by 4 at 0 μm/m, and it is divided by 5.5 at 100 μm/m. This progressive closure of gas pathways is the signature of micro-cracking, which is already present initially, at 0 μm/m. For P_c above 5 MPa, the decrease in K_{gas} with increasing P_c is parallel at 0 and 100 μm/m, hinting at identical gas pathway closure: the main difference is for P_c between 1 and 5 MPa, which corresponds to the closure of the sole micro-cracks created by splitting. Similarly, for UHPFRC, the sensitivity of K_{gas} to P_c is within the range 1–5 MPa: for P_c above 5 MPa, K_{gas} remains almost unchanged, as UHPFRC does not exhibit initial micro-cracks or defects. For both OC and UHPFRC, the sensitivity of K_{gas} to confinement is maximal in the range of confining pressures corresponding to the closure of cracks initiated by the splitting test (i.e. for $P_c = 1$ to 5 MPa).

A previous theoretical and experimental study [13] has shown that the sensitivity to confinement is related to the crack aspect ratio. Let then consider that the OC exhibits an initial heterogeneous cracking. The closure of these cracks occurs at different confining pressures, which justifies the decrease of gas permeability in the whole range of applied confining pressures (P_c = 1–30 MPa). On another hand, tensile loading (due to the Brazilian test) induces a sensitivity of K_{gas} to confining pressure, which is only visible in a narrow range of loading (between 1 and 5 MPa): this is attributed to a more homogenous cracking (in term of cracks aspect ratio and orientation).

3.5. Consequences for the protection of aging containment structures of nuclear reactors

This study has shown that after partial to full drying, diffuse damage and localized cracking, the UHPFRC proposed by Lafarge company is able to retain sufficiently low gas transport properties (gas permeability $K_{gas} = 10^{-18}$ to 10^{-17} m^2), so as to remain in the "very high" to "high" durability range of concretes, as proposed by [7]. Despite accelerated aging (imposed by drying, diffuse or localized damage), the sensitivity of UHPFRC permeability to mechanical loading (i.e. confining pressure) changes is also very limited. Further validation of this material for increasing the durability of containment structures of nuclear reactors requires changing the scale, to a structural level, by analyzing the durability of entire UHPFRC slabs glued on actual containment walls, which will be done in further research.

4. Conclusion

This experimental study has focused on a Fibered Ultra High Performance Concrete (UHPFRC) designed to be affordable for Civil Engineering applications. Our aim was to investigate its durability after progressive accelerated aging: partial drying, 105 °C oven-drying, 200, 300 or 400 °C heat-treatment and progressive splitting (by a Brazilian test). UHPFRC is compared to a standard mortar (M1) and to an ordinary concrete (OC). Our key experimental tool to assess durability is gas permeability under varying confinement, coupled to porosity measurement under varying confinement, MIP and SEM analysis to assess microstructure changes.

4.1. Basic durability assessment

Whereas usual UHPFRCs comprise pozzolanic additions and are cured thermally, this UHPFRC is not, and it is significantly more porous (by 9–10%). Its porosity places it in the "good durability range". As a durability indicator, porosity alone is not sufficiently reliable for UHPFRC. Indeed, 74% of UHPFRC porosity comprises pores smaller than 4 nm, i.e. located within the C–S–H. From a gas transfer point of view, 105 °C oven-dried UHPFRC lies in the range of "very high durable materials", with an average $K_{gas} = 10^{-18}$ m^2. By directly assessing the ability of fluid transport through the porous medium, gas permeability describes a better durability for UHPFRC than porosity alone.

4.2. Effect of accelerated aging on concrete durability

Diffuse damage produced by heat-treatment up to 400 °C features limited de-bonding at the fiber/paste interface, which increases its gas permeability up to 10^{-17} m^2 at 6 MPa confining pressure P_c: this is significantly smaller than for OC or for mortar M1, which K_{gas} increases respectively by 13 and 37 times at $P_c = 6$ MPa when compared to the dry reference state (105 °C oven-drying). Simultaneously, porosity under confinement increases from 9 to 12% (at $P_c = 2$ MPa) after 400 °C heat-treatment.

Finally, from splitting test data, fibers are shown to be very efficient to provide UHPFRC with enhanced tensile resistance. Simultaneously, gas permeability of UHPFRC remains virtually identical, while sustaining more than 300 μm/m tensile strain; on the opposite, OC sustains ca. 100–150 μm/m and is more sensitive to P_c changes. For both OC and UHPFRC, the main decrease in K_{gas} is observed at low confinement (1–5 MPa), which is attributed to the closure of micro-cracks created by progressive splitting.

Acknowledgments

This research has been supported by the National Natural Science Foundation of China (under Grant n.51109069), and by the Program for Changjiang Scholars and Innovative Research Team in University.

References

[1] C. Ozyildirim, Evaluation of ultra-high-performance fiber-reinforced concrete, Contract report n.73677, Virginia Center for Transportation/Innovation and Research, August 2011.
[2] L. Sorelli, G. Constantinides, F.J. Ulm, F. Toutlemonde, The nano-mechanical signature of Ultra High Performance Concrete by statistical nano-indentation techniques, Cem. Concr. Res. 38 (2008) 1447–1456.
[3] P. Richard, M. Cheyrezy, Reactive Powder Concretes With High Ductility and 200–800 MPa Compressive Strength, American Concrete Institute, 1994. 507–518 (SP 144–24).
[4] P. Richard, M. Cheyrezy, Composition of reactive powder concretes, Cem. Concr. Res. 25 (7) (1995) 1501–1511.
[5] D. Corvez, Bétons Fibrés Ultra Performants de la gamme Ductal®: De la matrice optimisée à la structure durable, Internal report, Lafarge (www.lafarge.fr), 2011.
[6] V. Baroghel-Bouny, K. Kinomura, M. Thiery, S. Moscardelli, Easy assessment of durability indicators for service life prediction or quality control of concretes with high volumes of supplementary cementitious materials, Cem. Concr. Compos. 33 (2011) 832–847.
[7] V. Baroghel-Bouny, Conception des bétons pour une durée de vie donnée des ouvrages—Maîtrise de la durabilité vis-à-vis de la corrosion des armatures et de l'alcali-réaction—Etat de l'art et guide pour la mise en oeuvre d'une approche performantielle et prédictive sur la base d'indicateurs de durabilité, Scientific and

Technical Report of the French Civil Engineering Association, AFGC, Bagneux, July 2004, (252 pp.).
[8] C.A. Davy, F. Skoczylas, J.D. Barnichon, P. Lebon, Permeability of macro-cracked argillite under confinement: gas and water testing, Phys. Chem. Earth A/B/C 32 (2007) 667–680.
[9] M. Lion, F. Skoczylas, B. Ledésert, Determination of the main hydraulic and poro-elastic properties of a limestone from Bourgogne, France. M Lion, F Skoczylas, B Ledésert, Int. J. Rock Mech. Min. Sci. 41 (2004) 915–925.
[10] X.T. Chen, C.A. Davy, J.F. Shao, F. Skoczylas, Experimental and micro-mechanical analysis of the mechanical and transport properties of mortar containing heat-induced micro-cracks, Cem. Concr. Compos. 32 (2010) 678–685.
[11] X.T. Chen, C.A. Davy, F. Skoczylas, J.F. Shao, Effect of heat-treatment and hydrostatic loading upon the poro-elastic properties of a mortar, Cem. Concr. Res. 39 (2009) 195–205.
[12] X.T. Chen, G. Caratini, C.A. Davy, D. Troadec, F. Skoczylas, Coupled transport and poro-mechanical properties of a heat-treated mortar under confinement, Cem. Concr. Res. 49 (2013) 10–20.
[13] E. Lemarchand, C.A. Davy, L. Dormieux, W. Chen, F. Skoczylas, Micromechanics contribution to coupled transport and mechanical properties of fractured geomaterials, Transp. Porous Media 79 (3) (2009) 335–358.
[14] C. Vernet, J. Lukasik, E. Prat, Nanostructure, porosity, permeability and diffusivity of UHPC, International Symposium on High-Performance and Reactive Powder Concretes, Sherbrooke, Canada, 2000.
[15] X.T. Chen, Effet du chauffage sur le comportement mécanique et poro-mécanique de matériaux cimentaires—propriétés hydrauliques et changements morphologiques, (PhD thesis) , 2009.
[16] H. Meziani, F. Skoczylas, An experimental study of the mechanical behaviour of a mortar and its permeability under deviatoric loading, Mater. Struct. 32 (1999) 403–409.
[17] W. Chen, J. Liu, F. Brue, F. Skoczylas, C.A. Davy, X. Bourbon, J. Talandier, Water retention and gas relative permeability of two industrial concretes, Cem. Concr. Res. 42 (2012) 1001–1013.
[18] A. Spasojevic, Structural implications of ultra-high performance fibre-reinforced concrete in bridge design, (PhD Thesis) EPFL, Lausanne, Switzerland, 2008. (285 pp.).
[19] ANDRA, Dossier 2005: référentiel des matériaux d'un stockage de déchets à haute activité et à vie longue, Tome 2: matériaux cimentaires, Document Interne ANDRA n° CRPASCM040015T2_A2005, 2005, (in French).
[20] G. Orange, J. Dugat, P. Acker, A new generation of UHP concrete: Ductal®. Damage resistance and micromechanical analysis, Proc. of the 3d Internat. RILEM Workshop, HPFRCC3-1999, 1999, pp. 101–111.
[21] P. Mounanga, Etude expérimentale du comportement de pâtes de ciment au très jeune âge: hydratation, retraits, propriétés thermophysiques, Thèse de doctorat de l Université de Nantes, 2003. (PhD Thesis, in French).
[22] G.W. Scherer, J.J. Valenza II, G. Simmons, New methods to measure liquid permeability in porous materials, Cem. Concr. Res. 37 (2007) 386–397.
[23] W.V. Kayser, Temperature dependence of the surface tension water in contact with its saturated vapour, J. Colloid Interface Sci. 56 (1976) 622–627.
[24] P.J. McDonald, V. Rodin, A. Valori, Characterisation of intra- and inter-C–S–H gel pore water in white cement based on an analysis of NMR signal amplitudes as a function of water content, Cem. Concr. Res. 40 (12) (2010) 1656–1663.
[25] F. Brue, C.A. Davy, F. Skoczylas, N. Burlion, X. Bourbon, Effect of temperature on the water retention properties of two high performance concretes, Cem. Concr. Res. 42 (2012) 384–396.
[26] F. Lea, The Chemistry of Cement and Concrete, J. Wiley & Sons Ed, 1998.
[27] J. Bear, Dynamics of Fluids in Porous Media, Dover Publication Inc., NY, 1988.
[28] F.A.L. Dullien, Porous Media, Fluid Transport and Pore Structure, 2nd edition Academic Press, San Diego, 1992.
[29] E. Dana, F. Skoczylas, Experimental study of two-phase flow in three sandstones. I. Measuring relative permeabilities during two-phase steady-state experiments, Int. J. Multiphase Flow 28 (2002) 1719–1736.
[30] H.F.W. Taylor, Cement Chemistry, 2nd edition Telford Publishing, London, 1997.
[31] K. Holschemacher, T. Mueller, Y. Ribakov, Effect of steel fibers on mechanical properties of high-strength concrete, Mater. Des. (ISSN: 0261-3069) 31 (5) (May 2010) 2604–2615, http://dx.doi.org/10.1016/j.matdes.2009.11.025.